Atmospheric Research 247 (2021) 105158

Contents lists available at ScienceDirect

Atmospheric Research

journal homepage: www.elsevier.com/locate/atmosres

A modeling study of the impact of stratospheric intrusion on ozone enhancement in the lower troposphere over the Hong Kong regions, China

Kaihui Zhao[a], Cheng Hu[b,*], Zibing Yuan[a], Danni Xu[a], Shu Zhang[a], Huihong Luo[a], Jinting Wang[d], Rongsheng Jiang[c]

[a] School of Environment and Energy, South China University of Technology, Guangzhou, China
[b] College of Biology and the Environment, Joint Center for sustainable Forestry in Southern China, Nanjing Forestry University, Nanjing 210037, China
[c] Yale-NUIST Center on Atmospheric Environment, International Joint Laboratory on Climate and Environment Change (ILCEC)/Collaborative Innovation Center on Forecast and Evaluation of Meteorological Disasters (CIC-FEMD), Nanjing University of Information Science & Technology, Nanjing, China
[d] Xianyang Meteorological Bureau, Xianyang, Shaanxi Province, China

ARTICLE INFO

Keywords:
Stratospheric intrusion
Ozone
WRF-Chem
The South China region

ABSTRACT

Stratospheric intrusion is of great importance to transporting ozone (O_3)-enriched air from stratosphere into the middle and lower troposphere. The Weather Research and Forecasting model coupled with Chemistry (WRF-Chem) was employed to simulate a typical stratospheric intrusion episode occurring on March 24, 2010 and examine the impact of stratospheric intrusion on the O_3 enhancement in the lower troposphere. An upper boundary condition scheme was applied to the simulations to overcome the limitation of WRF-Chem in which O_3 chemistry in the stratosphere is not included. The simulations were evaluated with various observational data including O_3 sounding, surface O_3, as well as the European Centre for Medium-Range Weather Forecasts (ECMWF) ERA-Interim reanalysis data. The WRF-Chem showed reasonable performance on simulating the meteorological processes that control the stratospheric intrusion. Several findings were identified from the detailed analyses of the modeling results. First, the subtropical high-level jet was responsible for this stratospheric intrusion event. When Hong Kong was located at the south side of the subtropical jet where subsidence was dominated, the O_3-enriched air was transported from stratosphere to troposphere. Second, the stratospheric intrusion caused substantial enhancement of O_3 with the maximum O_3 concentration higher than 80.0 ppbv in the lower above the atmospheric boundary layer in the Hong Kong region. Finally, the process analyses (PA) method is performed to quantify the impact of stratosphere intrusion on the O_3 enhancement in the lower troposphere. The PA result illustrates that a substantial increase in the lower troposphere O_3 is highly associated with vertical transport from the upper troposphere. These results indicated important role of stratospheric intrusion on O_3 enhancement events and more observations are advised to better constrain and quantify its effects.

1. Introduction

As a critical trace gas in the atmosphere, stratospheric ozone (O_3) accounts for about nine-tenth of the total atmospheric column and acts as a shield to protect life on Earth from harmful ultraviolet radiation (Sillman, 2014; Skerlak et al., 2014). When compared with the stratospheric O_3, the amount of tropospheric O_3 is much less, while it plays a critical role in radiative forcing (Brasseur et al., 1998; Lacis et al., 1990). Many studies have illustrated that high concentrations of surface O_3 is of great concern due to its detrimental effects on human health, natural ecosystems, and climate change (Ainsworth et al., 2012; Chameides et al., 1999; Krupa and Manning, 1988; Westervelt et al., 2019; Zhang et al., 2016). O_3 is also a greenhouse gas with strong absorption of solar radiation at wavelength of 200-300 nm (Dickinson and Cicerone, 1986). In addition, the main sources of OH radicals are the photolysis of O_3 which can start many oxidation reactions sequences in the troposphere (Lanzendorf et al., 2001). Hence, the study of O_3 enhancement mechanisms, especially for lower troposphere is of great importance.

Photochemical reaction plays a critical role in controlling O_3 budget in the troposphere. It is well known O_3 can been produced by a series of photochemical reactions between its precursors, volatile organic compounds (VOCs) and nitrogen oxides (NO_x, sum of nitric oxide (NO) and nitrogen dioxide (NO_2)), in the presence of conducive meteorological conditions such as high temperature, strong solar radiation, weak winds, and stable atmospheric boundary layer (Logan, 1989; Zhao

* Corresponding author.
E-mail address: nihaohucheng@163.com (C. Hu).

https://doi.org/10.1016/j.atmosres.2020.105158
Received 2 February 2020; Received in revised form 20 July 2020; Accepted 22 July 2020
Available online 26 July 2020

et al., 2019). Extensive studies have proved that photochemical productions act as one of the major sources of O_3 in troposphere (e.g., Fishman and Crutzen, 1978; Ling et al., 2013; Penkett et al., 2004; Singh and Sloan, 2006; Vieno et al., 2008; Zhao et al., 2019). Since preindustrial times, anthropogenic emissions have contributed 40-65% of increase in tropospheric O_3 through photochemical reactions (Horowitz, 2003; Mickley et al., 2001). Furthermore, local photochemical productions play a dominant role in the O_3 National Ambient Air Quality Standard (NAAQS) exceedance events in presence of conducive meteorological conditions such as heat-wave weathers (e.g., Lei et al., 2016; Wang et al., 2009; Zhao et al., 2019). To better understand the tropospheric O_3 formation mechanisms, several studies have been made to identify O_3 formation regimes (e.g., Derwent, 1990; Kim et al., 2009), the O_3-precursor nonlinearity (e.g., Sillman et al., 1990; Sillman, 1995), and the relative impact of photochemical reactions (e.g., Pu et al., 2017; Zhao et al., 2019). Both the spatial-temporal variation in tropospheric O_3 and occurrence of NAAQS O_3 exceedance episodes have been studied (Cooper and Peterson, 2000; Zhao et al., 2019). Among these studies, the tropospheric O_3 and its formation mechanism has been widely investigated.

Regional transport is the second key factor in modulating O_3 abundance in the troposphere. Extensive field campaigns and numerical models were developed to investigate the impacts of transports on O_3 evolution events. The Pacific Exploratory Missions (PEM-West) and the Transport and Chemical Evolution (TRACE-P) were among the representative field campaigns of measuring the air pollutants, which transported from the Asian boundary layer and over the North Pacific Ocean (e.g., Blake, 2003; Hoell et al., 1997). A global three-dimensional Lagrangian chemistry-transport model is applied to investigate the formation and transportation of the Asian plumes during the Intercontinental Transport and Chemical Transformation (ITCT) and Intercontinental Chemical Transport Experiments (INTEX-B) field campaigns (Derwent et al., 2004). These observational data provide convincible evidence that the long-range transport of both O_3 and its precursors from Asia shows an nonnegligible role in the O_3 budget in Europe and North America. Due to the substantial economic and industrial development in East Asia (Chan and Yao, 2008; Richter et al., 2005), the long-range transport from East Asia shows a significant impact on the surface O_3 enhancement in the western United States (US) during springtime (e.g., Cooper et al., 2010; Jacob et al., 1999). Several studies also pointed out that the long-range transport of biomass burning from Southeast Asia play a key role in contributing for the O_3 enhancement in the lower troposphere during springtime in Southeast China (Chan et al., 2000a b; Lam et al., 2005; Liang et al., 2002; Liang et al., 2004; Oh et al., 2010).

Stratospheric intrusion represents another major source of O_3 in the troposphere (Holton et al., 1995; Stohl et al., 2003; Regener, 1957). A number of studies have been conducted to explore the mechanisms of stratosphere-troposphere exchange (hereafter STE) (Price and Vaughan, 1993; Schoeberl, 2003; Tang et al., 2011). Typically, stratospheric intrusions are identified by elevated O_3 concentrations, high values of potential vorticity (PV), and low relative humidity (i.e., less than 20%) (Ganguly, 2012; Greenslade et al., 2017; Iwabe et al., 2009). Several studies also noticed that tropopause folding is generally associated with jet stream, and upper-tropospheric frontogenesis is an important mechanism of stratospheric intrusion (Archer and Caldeira, 2008; Baray et al., 2012; Langford et al., 2012; Reed, 1955; Shapiro, 1980). Accurate quantification of stratospheric intrusion is crucial to determine the spatial and temporal variations of O_3 in the troposphere (Meul et al., 2018). Collins et al. (2000) identified an increase in the stratosphere intrusion contribution by around 37% to tropospheric O_3 by using a global chemistry transport model and their results indicate that the stratosphere intrusion plays an important role in the tropospheric O_3 budget in the future. The Atmospheric Chemistry and Climate Model Intercomparison Project (ACCMIP) models were applied to calculate STE flux from 1850 to 2100 and they hold that the O_3 increase can be attributed to a 40-150% increased stratospheric intrusion O_3 flux for the Representative Concentration Pathways (RCP) 8.5 (Young et al., 2013). Additionally, Griffiths et al. (2020) noticed that STE plays a critical role in controlling the tropospheric O_3 burden during the period of O_3 depletion brought about by the emission of chlorofluorocarbon. Several studies attempted to calculate the STE flux with the numerical models and their results illustrated that the STE flux of O_3 varied from 400 to 600 Tg/yr (Gettelman et al., 1997; Hsu et al., 2005; Stevenson et al., 2006). Meanwhile, a coupled tropospheric chemistry climate model CHASER (Sudo et al., 2002) was used to investigate the contribution of stratospheric intrusion to the budget of tropospheric O_3 from 1990 to 2100 (Sudo, 2003). The model results indicated that the stratospheric intrusion was responsible for 80% of O_3 change in the troposphere.

The O_3 data from satellite product have been made to diagnose the stratospheric intrusion (Olsen et al., 2000; Price et al., 1994). Several studies proved that NASA's high-resolution global reanalysis data, MERRA-2 is able to capture the evaluation of stratospheric intrusions and the horizontal resolution is nominally 50 km, the maximum resolution of a gridded dataset advised to identify features of a stratospheric intrusion (50 km or less; Büker et al., 2005; Lin et al., 2012; Ott et al., 2016), since it assimilates total column O_3 retrievals from the Ozone Monitoring Instrument (Levelt et al., 2006). However, lack of high spatiotemporal resolution observational data in the upper troposphere to the lower stratosphere (UTLS region) to the lower stratosphere makes it very difficult to quantify the contribution of stratospheric intrusion to O_3 in troposphere. In addition, due to the limitation of vertical resolution, the current global atmospheric chemistry models are not able to accurately describe the dynamic process of transporting O_3 from stratosphere to troposphere (Considine et al., 2008; Frédéric et al., 2013). Locatelli et al. (2015) illustrated that the stratosphere-troposphere exchange is largely improved by increasing the vertical layers from 19 to 39. Although the impact of stratospheric intrusion on tropospheric O_3 at global scale and mid- to high Northern Hemisphere latitudes have been extensively studied, the quantification of impact of stratospheric intrusion on tropospheric O_3 at tropical latitudes still remain a large knowledge gap (Barrett et al., 2019; Hegglin and Shepherd, 2009; Yang et al., 2016; Li and Bian, 2015).

Compared to studies on long-range transport of biomass burning, the importance of stratospheric intrusion in the O_3 enhancement is less investigated in Hong Kong. Hong Kong, located at the subtropical regions (22°18′N and 114°10′E), is highly influenced by summer monsoon circulations. Active deep convection provides a conducive meteorological condition for stratospheric intrusion in springtime such as upper-level troughs and cut-off lows. In the past decade, many extremely high O_3 enhancement events were noticed at the height of 2–4 km over Hong Kong during springtime. According to back-trajectory analysis and modeling studies, the long-range transport of biomass burning from Southeast Asia represents the main mechanism leading to the O_3 enhancement (e.g., Chan and Chan, 2000; Zhang et al., 2012). However, one study using multiyear records of ozonesondes at nine locations along the North Pacific coast, together with backward trajectories, investigated the characteristics of North Pacific tropospheric O_3. Their results suggest that the O_3 enhancement around 30°N was closely tied to stratospheric intrusion (Oltmans et al., 2003).

To study and quantify the impact of stratospheric intrusion on the enhancement of O_3 in the lower tropospheric at the tropical latitudes, a typical stratospheric intrusion event observed on 24 March 2010 in southeast China was chosen, during which ozone and meteorological observations from the ozonesondes data were used. In this study, the Weather Research and Forecasting/Chemistry (WRF-Chem) will be applied for the numerical modeling of this event with the finest grid spacing of 3 km and 46 vertical layers. An upper boundary condition (UBC) scheme is also used to overcome the shortage that WRF-Chem does not have the capability of simulating O_3 in the stratosphere. These observations together with ECMWF re-analysis data are applied to

evaluate the model performance on simulating meteorological fields and chemical species. Process analysis (PA) was performed to quantify the impact of stratospheric intrusion on O_3 enhancement in the lower troposphere over the Hong Kong regions. The objectives of this study, therefore, are to: 1) identify the physical mechanism which governs the stratospheric intrusion of O_3 in Hong Kong; 2) demonstrate the capability WRF-Chem in simulating the stratospheric intrusion process; 3) quantify the impact of stratospheric intrusion and compare its contribution with local chemical productions to the O_3 enhancement at the 2-4km high over the Southeast China coastal regions during the stratospheric intrusion event in springtime.

2. Methodology and data

2.1. Model setup and configurations

The WRF-Chem model (version 3.7.1), which fully coupled regional numerical weather prediction with chemistry, was used in this study (Grell et al., 2005). In the online system, both the same horizontal grids and vertical coordinate were applied into the meteorological and chemical modules. Thus, the deviation from the interpolation of the off-line model is avoided. The WRF-Chem has been successfully used in the real-time forecast of weathers and air quality, field campaign design, aerosol-cloud interactions, and climate change research (Chuang et al., 2011; Fast et al., 2014; Hu et al., 2019; Pfister et al., 2017). To well simulate the stratospheric intrusion in our study area, WRF-Chem simulations were conducted over three nested-domains at grid-spacing of 27km, 9km, and 3km with grid points of 140 × 130, 130 × 118, and 118 × 106, from the outermost to innermost domains, respectively (Fig. 1). The outermost domain covers the southeast China and the innermost domain includes the Hong Kong and surrounding regions. Forty-six vertical levels from 1000 hPa to 50 hPa were applied with the lowest level about 44 meters above the surface layer and about 400 m vertical resolution in the UTLS. Based on our case study for the O_3 enhancement event, four-day simulations starting from 06 UTC on March 21, 2010 were conducted over the three nested domains, which will be shown and discussed in Results Section. The first 24-h simulations are considered as a spin-up time.

The initial and lateral boundary meteorological conditions are provided by the National Centers for Environmental Prediction (NCEP) analysis data, Final Global Data Assimilation System (GDAS) data 1° × 1° and 6 h of horizontal spatial and temporal resolution, respectively. The initial and lateral conditions for chemical species are produced from the outputs of the Model for Ozone and Related Chemical Tracers, Version 4 (MOZART, Emmons et al., 2010) with horizontal resolutions of 1.9° × 2.5° and 56 levels in the vertical direction provided initial and spatial/temporal chemical boundary conditions. The resolution of the UTLS for MOZART outputs is about 470 m.

Table 1
WRF-CHEM model configuration.

Basic equations	Non-Hydro mode	Reference
Microphysics	Lin scheme	Lin et al. (1983)
Longwave radiation	Rapid Radiative Transfer Model (RRTM)	Mlawer et al. (1997)
Shortwave radiation	Goddard Shortwave scheme	Chou (1995)
Boundary-layer	Yonsei University Scheme (YSU) scheme	Hong et al. (2006)
Chemistry	Fast-J photolysis scheme	Wild et al. (2000)

As noted above, we added the upper boundary condition scheme, developed by Barth et al. (2012), to overcome the shortage that WRF-Chem does not have the capability of simulating O_3 in the stratosphere. The key chemical species concentrations are set to climatological averages in this scheme and it can adjust key chemical species (ie., O_3, nitrogen oxides (NO, NO_2), nitric acid (HNO_3), methane (CH_4), monoxide carbon (CO), Nitrous Oxide (N_2O), nitrogen oxide (N_2O_5)) with the global atmospheric chemical model result. These values are overwritten as defined in the idealized chemical profile from 50 hPa down to the tropopause using a 10 day time constant. The tropopause height is computed from temperature from WACCM, which is used in the application of the upper boundary condition in the WRF-Chem model (Barth et al., 2012; Lamarque et al., 2012). This upper boundary condition scheme will enable the WRF-Chem model to accurately simulate the STE processes and to quantify the impact of stratosphere intrusion on the concentration of chemical species in the troposphere. The parameterization schemes employed in this study are list in Table 1.

Anthropogenic emissions are taken from the 2010 Model Inter-Comparison Study for Asia (MICS-Asia), which was developed by Tsinghua university, China (Lei et al., 2016; Li et al., 2015), the Multi-resolution Emission Inventory for China (MEIC), Regional Emission inventory in Asia (REAS2), Peking University (PKU)-NH3 inventory, Clean Air Policy Support System (CAPSS), and Argonne National Laboratory (ANL-India). The emission inventories consist of five categories (i.e., power plants, industry, residential, transportation, and agriculture) during data processing with a spatial resolution of 0.25°.

2.2. Observational and supporting data

The vertical profiles of observation data were measured at Hong Kong Observatory site (HKO, 22.31°N , 114.17°E, 66 m above sea level), which mainly contained O_3 and conventional meteorological variables including temperature, relative humidity, and wind speed. For the O_3 partial pressure, it was measured with interval range of 10 m and will be used to verify the WRF-Chem simulated vertical profiles. Data

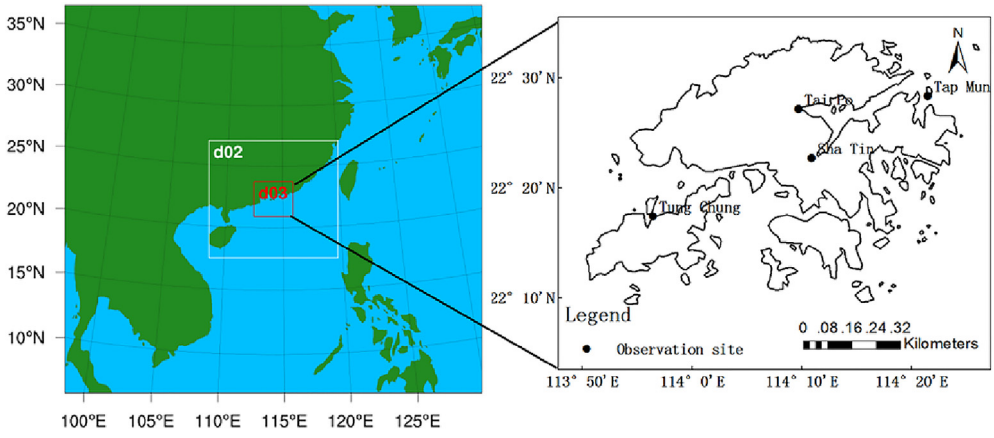

Fig. 1. Settings of three domains in WRF-Chem and four observation sites in Hong Kong.

are available once a week around 1400 local standard time (LST) and span from 2004 to 2018. The ozonesonde uses the Electrochemical Concentration Cell (ECC) developed by Vaisala Company in Finland. The ECC is based on an electrochemical method with two cells in Teflon (Gaudel et al., 2015). This instrument has been widely used to obtain the vertical distribution (Komhyr et al., 1985; Komhyr et al., 1989). In addition, the surface weather map and the monthly tropopause height was provided by Hong Kong Observatory which is available at http://envf.ust.hk/dataview/hko_wc/current/ and https://www.hko.gov.hk/en/publica/, respectively.

Meanwhile, the ERA-Interim reanalysis data from ECMWF will also be used to evaluate our model simulations, including wind speed, vertical velocity, potential vorticity and O_3. It spans from January 1979 to August 2019 with a temporal resolution of 6 hours, spatial resolution of 80 km, and has 60 levels in the vertical from the surface up to 0.1 hPa. The native data fields were interpolated on a $0.125^\circ \times 0.125^\circ$ grid. This dataset is available at https://apps.ecmwf.int/datasets/data. ERA-Interim has been widely used in the numerical studies of stratospheric intrusion events (Skerlak et al., 2014; Zanis et al., 2013). Since the O_3 data has been assimilated in ERA-Interim with a larger data set such as the Global Ozone Monitoring Experiment (GOME) O_3 profiles, the ERA-Interim O_3 product are in high consistence with O_3 data retrievals from a set of satellite instruments (Dragani, 2011). The boundary layer height (BLH) data was retrieved from the ERA-Interim dataset with spatial resolution of 0.125° during the period from 2004 to 2018.

2.3. Process analysis

As a post-processing tool, integrated process rate (IPR) analysis is used to quantify the relative contributions of individual physical process and chemical production for chemical species formation in the O_3 episodes (e.g., Gao et al., 2016; Huang, 2005; Jeffries and Tonnesen, 1994). The processes tendencies correspond to the accumulated values of each process per time step and grid which contains detailed information for each process in WRF-Chem (i.e., advection, deposition, vertical mixing, and chemistry). In this study, the IPR analysis is performed for the layers with substantial enhancement of O_3 concentrations as well as other two layers corresponding to the lower, middle, and upper portions of the troposphere for a certain time window that matches the launching time of O_3 sounding around 1-2 pm LST.

3. Results and discussion

3.1. Overview of stratospheric-intrusion O_3 enhancement in the lower troposphere

To understand monthly and annual variations of O_3 dynamics, the time-height cross-section plot of monthly mean O_3 profiles observation from the year of 2004 to 2018 is displayed in Fig. 2 measured by O_3 soundings at the Hong Kong observational site. Fig. 2a clearly shows the temporal and vertical variations in tropospheric O_3 over the Hong Kong, where the weather and climate are significantly influenced by the summer East Asia Monsoon (Liu et al., 2003; Zhou et al., 2013). It is clear there is strong O_3 gradient near the tropopause with the largest values in stratosphere and smallest values above ground level. Note that a significant O_3 enhancement (reached 60.0 ppb) is observed above the atmospheric boundary layer (ABL) top which is closely associated with a tongue-shape plume of high O_3 concentrations extending from the stratosphere during the springtime. Besides, a notable seasonal pattern of O_3 is observed that the O_3 concentration reached lowest value in summer and exceeded the highest value in fall within the ABL. The lowest value in summer is mainly related to summer East Asia Monsoon flows that the air flow was switched from the Asian continent to the South China Sea or the tropical Pacific which bring clean air to the south China coastal region (Chan et al., 1998). In addition, the O_3 increment in fall can be attributed to the regional transport from the Pearl River Delta region which brings polluted air to Hong Kong (Huang, 2005; Oltmans et al., 2003). Fig. 2b and 2c depict the vertical and temporal distribution of monthly mean O_3 excluding stratospheric intrusion occurs and only stratospheric intrusion occurs in Hong Kong. Here we defined the stratospheric intrusion event as the case when relative humidity (RH) is less than 20% and potential vorticity (PV) is larger than 1 potential vorticity unit (1 PVU, defined as 1.0×10^{-6} m^2 s^{-1} K kg^{-1}) (Beekmann et al., 1997; Brioude et al., 2007; Kim and Lee, 2010). We also noticed that O_3 enhancement in the lower troposphere is obviously weakened when the stratospheric intrusion event was excluded (Fig. 2b). Alternatively, O_3 concentrations with only stratosphere intrusion event reached 80 ppbv between the tropopause and the ABL (Fig. 2c) are much higher than those without stratosphere intrusion. Thus, we can conclude that the stratospheric intrusion plays a critical role in the O_3 enhancement in the lower troposphere. In general, the time-height cross-section plot of O_3 indicates that STE may be a key mechanism of determining temporal-spatial variations of O_3 in the troposphere during springtime. Similar phenomenon was also observed in other regions such as Europe and the United States (Moody et al., 1995; Oltmans et al., 2003).

Table 2 further presents a summary of the total numbers of O_3 enhancement cases observed at the layer of 2-4 km ABL, and the number of cases that are closely associated with stratospheric intrusion in springtime (March, April, and May) over Hong Kong during the period from 2004 to 2018. Here the O_3 enhancement case is defined as the case when O_3 concentration is larger than the climatological mean O_3 of 60 ppb since O_3 mixing ratios are strongly influenced by transport from the highly polluted Pearl River Delta region. The RH is coming from the sonde data and PV is extracted from ERA-Interim data. It is noted that stratospheric intrusion accounts for 36% of all O_3 enhancement events in springtime over the period of 2004-2018. In a previous study, the fraction of 10-20 trajectories starting between 5500 m and 13500 m that satisfy the STE criterion in Southeast China in one year which can further strengthen our conclusions (Stohl, 2001). Note here the stratospheric intrusion is much less investigated when compared with biomass burning in mainland Southeast Asia, which has been identified as the major source causing O_3 enhancement in the lower troposphere over the Hong Kong region (Chan et al., 2003; Zhang et al., 2012), and these findings conclude the nonnegligible role of stratospheric intrusion on ABL O_3 enhancement events.

3.2. A typical case of stratospheric-intrusion driven O_3 enhancement

A typical case with O_3 concentrations higher than 85.0 ppb at the 2.5 km ABL was observed in Hong Kong on March 24th, 2010, which provides a unique opportunity to quantify stratospheric-intrusion driven O_3 enhancement. To display the vertical structure for O_3 enhancement and other meteorological parameters for this event, vertical profiles of temperature, O_3, relative humidity, and wind speed measured by the ozonesonde at Hong Kong Observatory located at Kings Park (22.31°N, 114.17°E) are illustrated in Fig. 3. These four variables display different vertical profiles in the troposphere. O_3 is increasing with altitude and shows a large fluctuation extending from surface to the tropopause. A similar increasing trend is seen in the wind-speed profile with its maximum value (> 35.0 m s^{-1}) at the 12-14 km height. The air with O_3 concentration higher than 80.0 ppb and relative humidity less than 20% was extended from the tropopause (i.e., 17 km) downward to 5km ABL. Since the stratospheric air mass is relatively weak turbulent mixing with tropospheric air, the intruded O_3-enriched air with low relative humidity measured by ozonesonde can be identified as the evidence of stratospheric intrusion (Sørensen and Nielsen, 2001). Thus, we conclude that the substantial increase in the lower troposphere O_3 is highly associated with the stratospheric intrusion. Meanwhile, low-level clouds indicated by relative humidity nearly at 80% formed near the top of the boundary layer or bottom of the entrainment zone which identified by the temperature profile inversion at

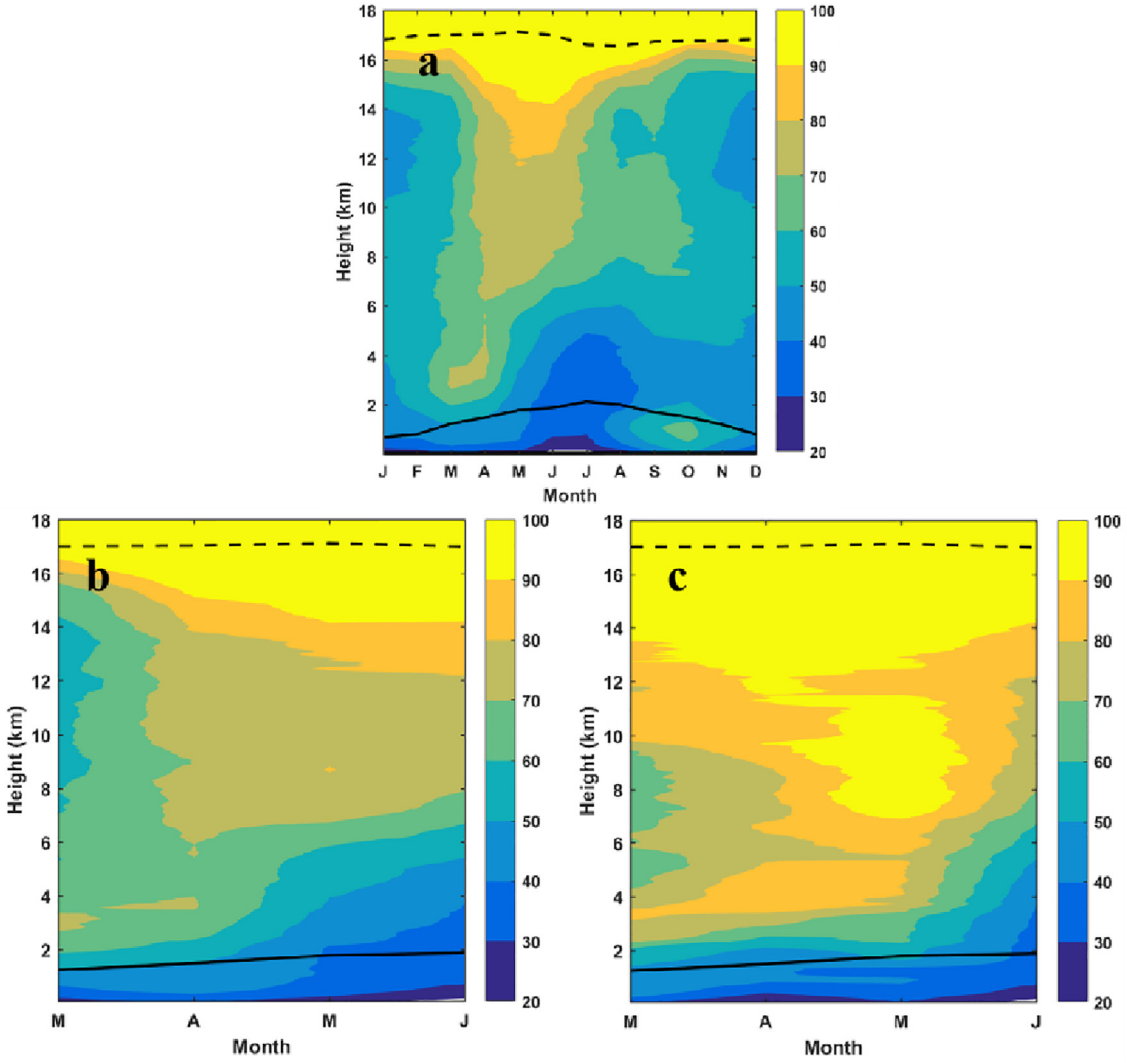

Fig. 2. Vertical and temporal distribution of monthly mean O_3 in Hong Kong (a) during 2004-2018, (b) monthly mean O_3 excluding stratospheric intrusion occurs during springtime (c) monthly mean O_3 for only stratospheric intrusion occurs during springtime. Note the dashed dark line is the average tropopause height and the solid dark line is the average BLH. (The O_3 data and monthly tropopause height was provided by Hong Kong Observatory; The BLH data was retrieved from the ERA-Interim dataset).

about 2 km. With such a strong stable layer (i.e., entrainment zone), the O_3-enriched air with high momentum was blocked to be penetrated through the entrainment zone. As a result, a strong gradient of O_3 and a low-level jet were developed simultaneously above the top of the atmospheric boundary layer.

The two reasons for choosing this event are mainly related to its typical vertical structure (Fig. 3). One reason is that the air, with O_3 concentration higher than 100.0 ppb and relative humidity less than 20%, extended from the tropopause downward to the lower troposphere and satisfy the stratospheric intrusion criterion. Another important reason is that a large change of O_3 from 25 to near 90 ppb around 3 km was observed, resulting from the O_3 enhancement associated with stratospheric intrusion, which is similar with the vertical and temporal distribution of monthly mean O_3 in Hong Kong during 2004-2018 (Fig. 2a and Fig. 1s). It will be discussed in details in the following parts. This event is representative of the general phenomenon of O_3 occurrence, and has significance for the future quantification and assessment of stratospheric intrusion in Hong Kong during springtime.

Based on the weather dynamics maps, we noticed a low-pressure system situated at the west side of Hong Kong and governed the weather over the Hong Kong and nearby regions at 1400 LST on March 24 2010 (Fig. 4b). A strong high-level jet was observed between 20°N and 30°N with the maximum wind speed higher than 50 $m{\cdot}s^{-1}$ around the jet core at the 300-hPa pressure level at 1400 LST (Fig. 4a). Here the clear sky was dominated over the region and strong divergence appeared at the upper portions of the troposphere (i.e., 300-150 hPa levels, see Fig. 4c). The divergence was calculated from GMS-5 Satellite data by Japan Meteorological Agency. High-level wind jet represents

Table 2
The total numbers of O_3 enhancement cases occurring at the layer of 2-4 km and the number of STE cases in springtime over Hong Kong during 2004 -2018.

Year	2004	2005	2006	2007	2008	2009	2010	2011	2012	2013	2014	2015	2016	2017	2018	total
2-4km > 60	9	5	4	6	4	5	5	4	6	4	4	8	8	8	6	86
STE	5	2	1	1	0	3	2	1	1	2	1	3	3	3	3	31

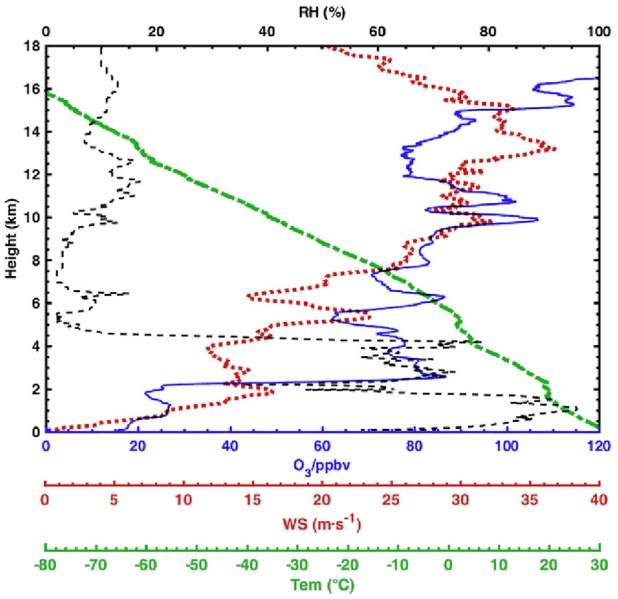

Fig. 3. The measured profiles of O_3 (blue solid line), temperature (green thick dashed-dotted line), relative humidity (black thin dashed line) and wind speed (red thick dashed line) below 18 km on March 24, 2010. (For interpretation of the references to color in this figure legend, the reader is referred to the web version of this article.)

one of important mechanisms driving stratospheric intrusion transporting O_3-enriched air from stratosphere to troposphere (Kim et al., 2002; Langford, 1999). Subsidence motion is developed at the south side of the subtropical jet stream (STJ), as a result of STJ evolution and the low-latitude vertical circulation (Blackmon et al., 1977; Langford, 1999).

3.3. Simulation of the stratospheric intrusion event

The WRF-Chem model will be used here to better explain and quantify this O_3 enhancement event, and as noted in Introduction Section, accurate representation of O_3 abundance or concentrations in the stratosphere is critical to assess impact of stratospheric intrusion on tropospheric O_3. The capability of simulating spatial and temporal variations of O_3 in the stratosphere is largely constrained given the fact that gas-phase chemical mechanism of O_3 formation in the stratosphere is not included in the WRF-Chem. To deal with the limitation, the UBC scheme proposed by Barth et al. (2012) was utilized by WRF-Chem to adjust O_3 concentrations in the stratosphere. Three-day simulations starting from 06 UTC (8 hours behind local standard time, LST) on March 22, 2010 were conducted over the three nested domains. The ozonesounding data are used to evaluate simulated vertical profiles of O_3, temperature, relative humidity, and wind speed at 1400 LST on March 24, 2010 (Fig. 5). To demonstrate how the UBC scheme improves O_3 predictions, both simulations with and without UBC scheme were evaluated with observations as displayed in Fig. 5a. The simulated O_3 concentrations were much higher than the observed values at the levels higher than 1.0 km when the UBC is not used. The positive prediction

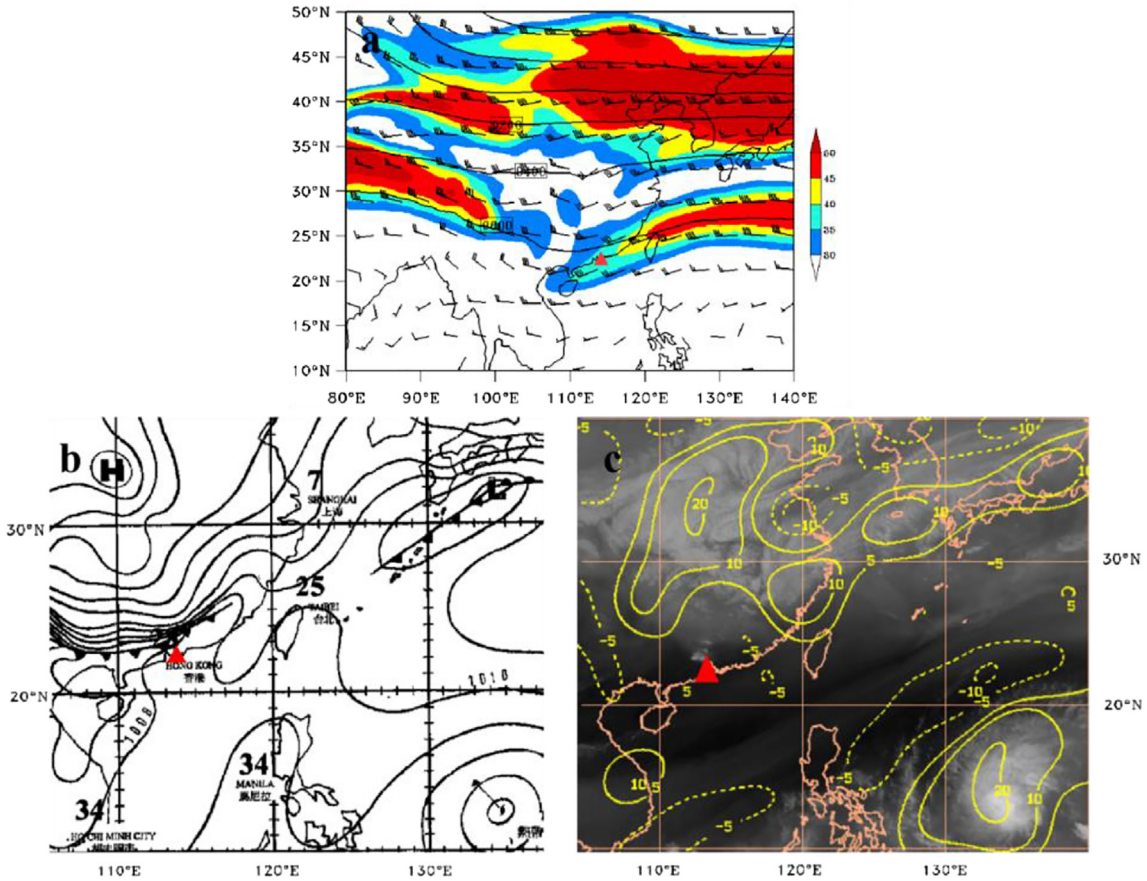

Fig. 4. (a) Horizontal wind field (shaded colors), geopotential height (black contour, units: m), and wind speed (black barb, units: m s^{-1}) from the ERA-Interim data at the 300-hPa level (b) surface weather map at 1400 LST on March 24 2010 (provided by Hong Kong Observatory) (c) the Japanese Geostationary Meteorological Satellite 5 (GMS-5) retrieved cloud coverage (shaded area) and divergence (contour) at the 300-150 hPa layers (provided by Japan Meteorological Agency) at 1400 LST on 24 March 2010 (Red triangle: Hong Kong location, 22.3°N, 114.2°E) (For interpretation of the references to color in this figure legend, the reader is referred to the web version of this article.)

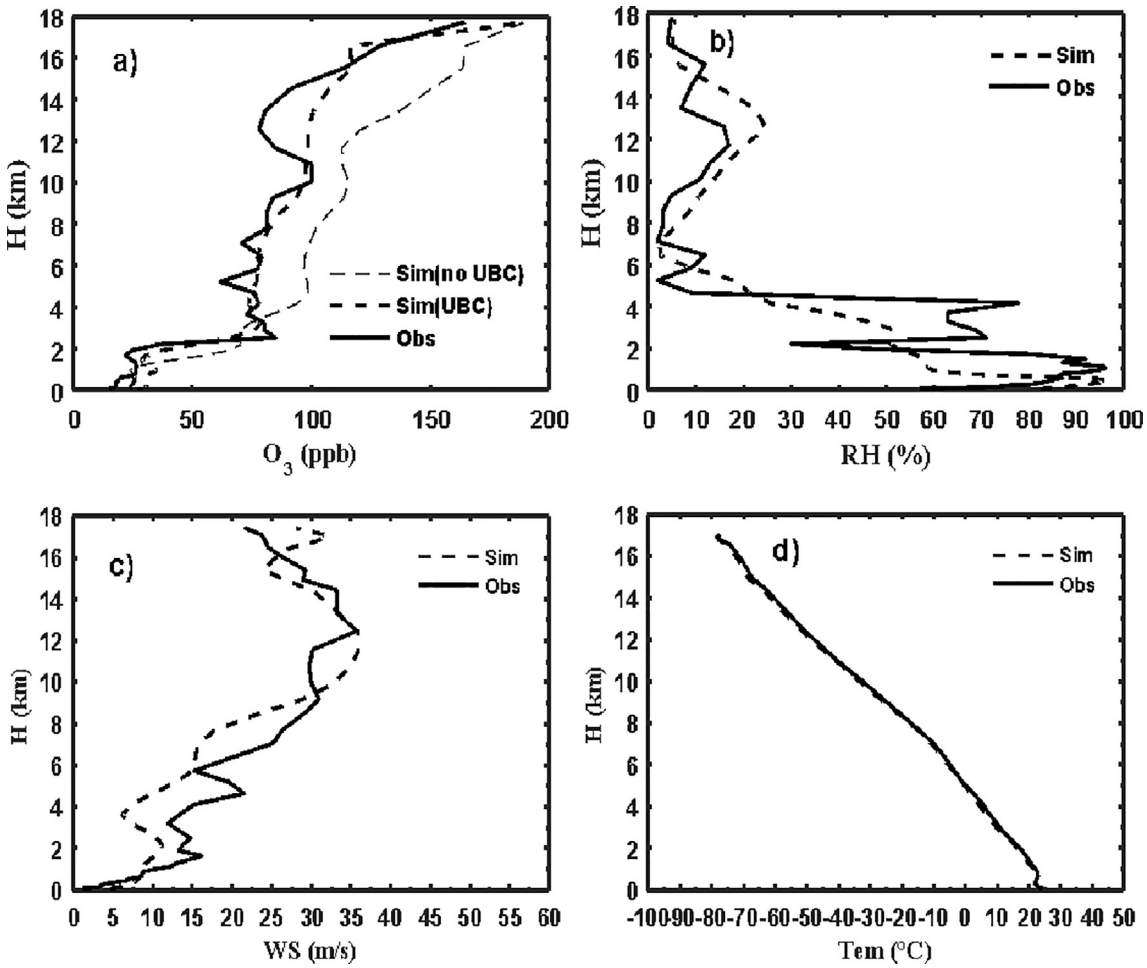

Fig. 5. A comparison of WRF-Chem simulated vertical profiles with observed a) O_3 (ppbv), b) relative humidity (RH, %), c) wind speed (WS, C), and d) temperature (Tem, ˚C) in Hong Kong at 1400 LST on March 24, 2010.

Table 3
Statistical comparisons between simulated and measured meteorological variables

	R^2	RMSE	MB
$O_{3\ (no\_UBC)}$	0.88	23.8	16.8
$O_{3\ (UBC)}$	0.92	18.7	11.7
RH	0.72	17.4	8.2
WS	0.86	4	-1.86
Tem	0.98	1.8	0.5

biases are closely associated with the unrealistic high O_3 concentrations in the stratosphere used by the WRF-Chem in the simulation without the UBC option, while simulated O_3 shows much better agreement with the ozonesonde data after the UBC scheme is applied. By using the UBC, the correlation coefficient (R^2) between simulated and observed O_3 increased from 0.94 to 0.96; the mean bias (MB) and root mean squared error (RMSE) reduced from 16.8 to 11.7 and from 23.8 to 18.7, respectively (Table 3). In addition, the impact of the UBC scheme on meteorological simulations is negligible and was not shown. These results give us confidence that our WRF-Chem setup can well capture the O_3 profiles.

The impact of the stratosphere intrusion on surface O_3 concentrations is illustrated further in the time-height cross-section plot of O_3 (Fig. 6). On March 22nd, the O_3-enriched air mass extended from the tropopause to 10.0 km with O_3 reaching 90.0 ppbv. One day later, the intrusion subsided to 6.4 km with its maximum value of 85.0 ppbv. On March 24nd, a pool of O_3 with concentration higher than 80.0 ppbv

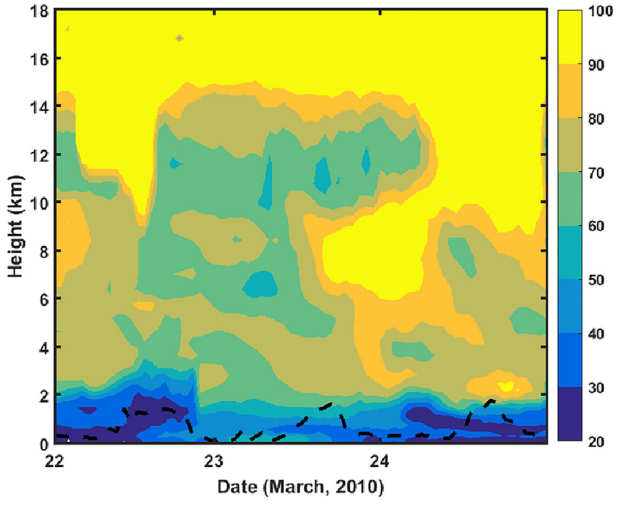

Fig. 6. Time-height cross section plot of simulated O_3 (O_3, ppbv) at Hong Kong during March 22–24 2010. Black line indicates model-estimated BLH.

appeared above the boundary layer, which was transported from stratosphere. Such processes indicate that WRF-Chem is able to well represent the development of the whole stratosphere intrusion event.

It is noted that a large O_3 jump with 50.0 ppbv was developed near the top of the ABL (i.e., about 2.5km ABL) in the simulations resulting from the O_3 enhancement associated with stratospheric intrusion. Such

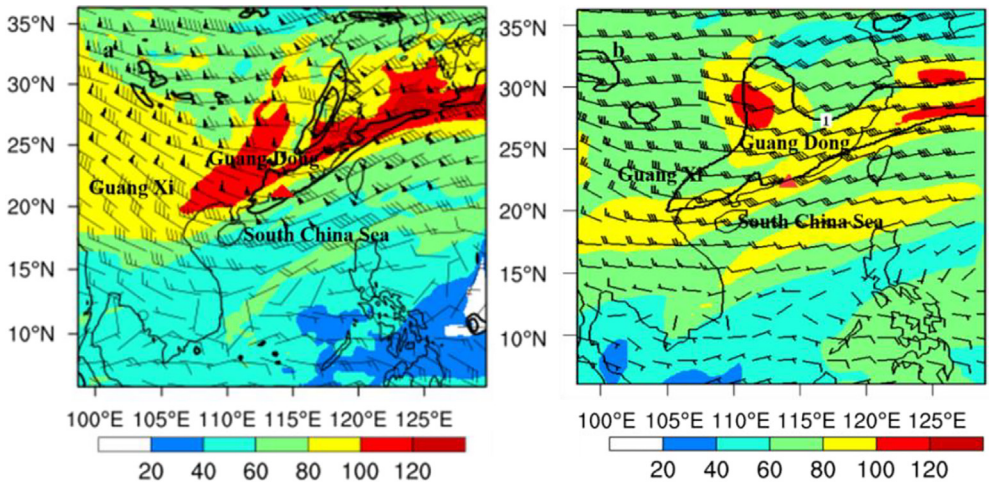

Fig. 7. A comparison of (a) WRF-Chem-simulated O_3, wind speed and potential vorticity (PV) with (b) ECMWF analysis data at the 300hPa level at 1400 LST on March 24,2010 (shaded colors: O_3; black contours: PV; black barb: wind speed; Red triangle: Hong Kong location, 22.3°N, 114.2°E). (For interpretation of the references to color in this figure legend, the reader is referred to the web version of this article.)

high O_3 enhancement may provide a large impact on the effectiveness of emission control measure application for alleviating severity of high concentrations of O_3. This is only true if the O_3 could be entrained into the boundary layer and reach the surface in the time of the event or following the intrusion event.

Comparison of WRF-Chem simulated O_3 and PV with the ECMWF reanalysis data at the 300hPa level, 1400 BTJ on March 24, 2010 was conducted in Fig. 7. The concentration and position of the ozone enhancement area from the model agreed well with the ECMWF reanalysis data. The high ozone concentration area has a significant distribution pattern of the southwest-northeastern band in the range of 20 ° N -35 ° N. The O_3 maximum center located at Guangxi (22° N, 103°E) and Guangdong (23°N, 114°E) province, and is more than 80.0 ppbv at 300hPa layer.

PV is a useful indicator to distinguish stratospheric air from tropospheric (Ganguly, 2012; Greenslade et al., 2017), the sharp transition between the high PV values in the stratosphere and the low PV values in the troposphere is then used to define the location of the dynamical tropopause. Stratosphere intrusion can favor a downward transport of high PV from the stratosphere to the troposphere (Ambaum, 1997; Ren et al., 2014). Thus, The high PV area had a good agreement with the O_3 distribution, corresponding to the characteristics of the stratospheric intrusion air. A westerly jet is also noticed in the range of 20°-30° N in Fig. 4 and the jet is much stronger in WRF-Chem simulation than ERA-Interim.

3.4. Physical factors of driving tropospheric intrusion

The WRF-Chem simulations are further combined with the sounding data to determine the key physical factors governing stratospheric intrusion. Fig. 8a and 8b depicts the latitude-pressure cross-section of WRF-Chem simulated O_3, PV, and wind speed at 14 LST on March 24, 2010 along the longitude of 114.17°E which passes through the HKO site. The model data was interpolated to this longitude. The vertical distribution of the O_3 enhancement area from the model agreed well with the ECMWF reanalysis data. A stratospheric intrusion process is identified by a tongue-shaped plume with O_3 concentration higher than 110 ppbv extending from the 200-hPa level (i.e., stratosphere) at 25°-30°N southward down to the 280-hPa level (i.e., troposphere) at 20°-25°N. The stratospheric intrusion of O_3 was closely associated with the STJ located at 25°-30°N near the 200-hPa level with the maximum wind speed higher than 50 $m{\cdot}s^{-1}$. The existence of STJ represents an important mechanism driving the tropopause folding (Gouget et al., 1996; Krishnamurti, 1961). The STJ is dominated by prevailing westerly winds over the subtropical region in the northern hemisphere and a strong vertical wind shear near the core of STJ is responsible for a large-scale subsidence at the south-hand side. The subsidence accompanied by the tropopause folding near the jet core brings O_3-enriched air from stratosphere downward to the troposphere.

A comparison of WRF-Chem-simulated latitudinal cross-sections of wind speed and vertical velocity with the ECWMF reanalysis data at 1400 LST on 24 March 2010 is depicted in Fig. 8c and 8d. Compared to the ECMWF reanalysis data, the WRF-Chem result shows a similar sink area from 200 hPa to 600 hPa between 20°-30°N. However, the WRF-Chem simulation depicts a lower vertical velocity with more perturbations due to the higher horizontal/vertical resolution applied in model simulation. A strong high-level jet was developed at 200 hPa and the wind speed at the STJ core reached 50 $m \cdot s^{-1}$. A strong sinking movement was observed between 20°-30°N developed at the south side of the STJ. Strong subsidence exceeds 0.6 Pa/s extended from 200 hPa to 600 hPa indicating a stratospheric intrusion process (Fig. 8c). In addition, an updraft airflow rises from surface to 600 hPa which lead to the large O_3 jump observed in Fig. 5.

3.5. Quantification of stratospheric intrusion on O_3 enhancement in the lower troposphere

Since it has been established in the previous discussion that contribution of stratosphere intrusion in Hong Kong was significant, to quantify stratospheric intrusion on O_3 enhancement in the lower troposphere, integrated process analyses will be further discussed by combing the simulation work in this section, and Domain 3 is chosen for process analysis calculation as defined in Fig. 1. The period of 11:00-15:00 LST was selected because the ozonesonde was launched at 14 LST and photochemical reactions for O_3 formation were the most active (Liu and Roy, 2015). Compared to the monthly mean O_3 in Fig. 2, the O_3 was enhanced substantially with the concentration higher than 80ppbv within the layer of 2-4km. The integrated process analyses were conducted for three different layers to quantify the contribution of stratospheric intrusion versus chemical production to O_3 enhancement at different heights in the troposphere. Compared to the climatology value, the three layers correspond to the lower layer (i.e., 2.5-4 km ABL), where O_3 experienced substantial enhancement; the middle layer (i.e., 4-10 km), where O_3 is close to the climatology value; and upper portions (i.e., 10-16 km) below the tropopause, where O_3 is much larger than the climatology value (Fig. 1S).

The hourly contributions from individual process tracked by the IPR method described in Section 2.3 are illustrated in Table 4. As expected, the results showed contributions from photochemical production were negligible in troposphere. Vertical transport (a sum of vertical advection and vertical diffusion) was the major process contributing to the increase in lower troposphere O_3 while horizontal advection (or transport) exported O_3 from the studied region. The O_3 change was the sum of vertical contribution, horizontal contribution and chemical

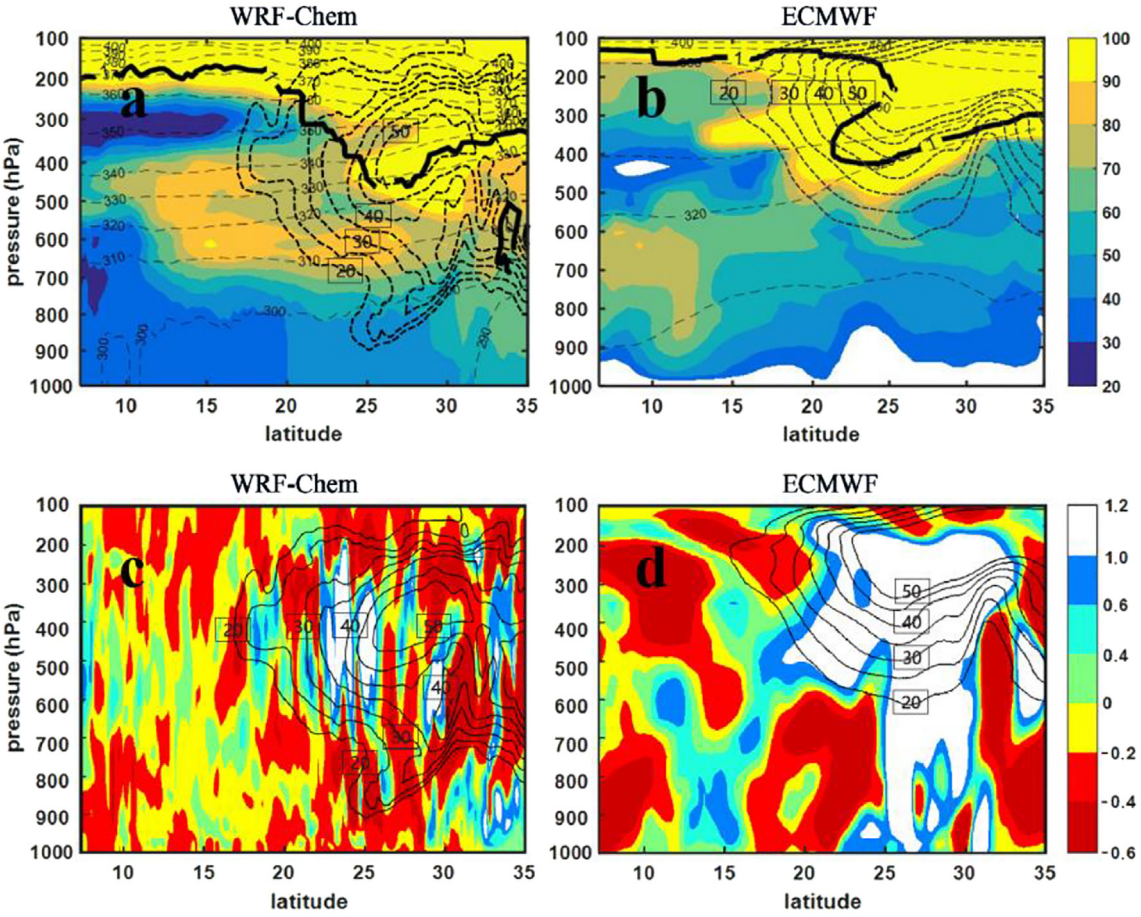

Fig. 8. A comparison of (a) WRF-Chem-simulated latitude-height cross section of O_3 (ppbv), potential vorticity (PV), wind speed (m s^{-1}) and potential temperature (K) with (b) ECMWF analysis data (shaded colors: O_3; heavy solid line: PV; heavy dashed lines: wind speed; dash-dot lines: potential temperature), (c) WRF-Chem-simulated latitudinal cross-sections of wind speed (m s^{-1}), and vertical velocity (Pa/s) at Hong Kong (114.17°E) at 14:00 LST on March 24, 2010 with (d) ECMWF reanalysis data (shaded colors: vertical velocity; contours: wind speed). (For interpretation of the references to color in this figure legend, the reader is referred to the web version of this article.)

Table 4
Comparisons of the O_3 change and the contribution of individual process and the net change for the period of 11:00-15:00 LST

height(km)	Vertical (ppbv·hr^{-1})	Horizontal (ppbv·hr^{-1})	Chemical (ppbv·hr^{-1})	Net (ppbv·hr^{-1})
2.5-4	17.3	-15.0	-0.4	1.9
4-10	11.0	-10.0	-0.1	0.9
10-16	22.0	-20.0	0.1	2.1

contribution. As shown in Table 4, the O_3 concentration increased 2.1 ppbv, 0.9 ppbv, and 1.9 ppbv during 11:00-15:00 LST at the upper portions, the middle layer, and the lower layer, respectively. The largest increment is mainly associated with large contribution of stratosphere intrusion. At the middle layer, the O_3 increment decreased to 0.9 ppbv due to the weakened downward transport process which corresponds to the lower O_3 concentrations, as shown in Fig. 8a. At the lower layer, the O_3 increment increased to 1.9 ppbv which was attributed to the strong stable layer observed at 2.5km (Fig. 3). The O_3-enriched air with high momentum was blocked to be penetrated through the stable layer. As seen in Fig. 8c and 8d, an updraft airflow rises from surface to 600 hPa which lead to the large O_3 jump. The produced O_3 through vertical transport averaged over the pre-defined region and studying time period was 17.3 ppbv·hr^{-1} from 2.5 km to 4 km, 11.0 ppbv·hr^{-1} from 4 km to 10 km and 22.0 ppbv·hr^{-1} from 10 km to 16 km. Alternatively, the horizontal transport plays a negative role from 2.5km to 16km. Through the process analysis, it is found that the vertical transport contributed the significant O_3 enhancement during the O_3 episode event. Since the net O_3 change is 0.9-2.1 ppbv/hr^{-1}, the accumulated contribution may reach to 21.6-50.4 ppbv in 24 hours. Thus, our results indicated that the stratosphere intrusion may play a critical role in O_3 enhancement in the lower troposphere over the Hong Kong regions during springtime. Compared the contribution of the transportation of biomass burning to the spring O_3 maximum, quantification of impact of the stratosphere intrusion still remains a large uncertainty.

4. Conclusions

A typical O_3 enhancement event driven by stratosphere intrusion was observed in Hong Kong on March 24, 2010. The WRF-Chem model was conducted to assess the impact of different factors (mainly a stratospheric intrusion) on O_3 enhancement in the lower troposphere over the Hong Kong. To improve model performance, the UBC scheme was employed to overcome the shortage that WRF-Chem does not have the capability of simulating O_3 in the stratosphere. A series of available observational data including ozonesonding data, surface observations and ECMWF re-analysis data are used to evaluate the model capability of simulating the stratosphere intrusion process.

Time-height cross-section plot of monthly mean O_3 measured by O_3 soundings at the Hong Kong observational site over the period from years 2004 to 2018 shows a significant O_3 enhancement reached 60.0 ppb above the atmospheric boundary layer top, which is likely

associated with the stratosphere intrusion during the springtime. Previous studies have identified the biomass burning from Southeast Asia as the major source causing O_3 enhancement in the lower troposphere over the Hong Kong region. However, both the statistical analysis of stratosphere intrusion case and seasonal variation of monthly O_3 indicate that the stratosphere intrusion may play a critical role in O_3 enhancement in the troposphere over Hong Kong. Compared to the ERA-Interim reanalysis data and ozonesonde data, the WRF-Chem model shows a good performance on the vertical distribution of temperature, relative humidity, wind speed and O_3 when using the Upper Boundary Condition scheme. The simulated O_3 shows much better agreement with the O_3 sounding data after the UBC scheme is applied. The stratospheric intrusion of O_3 was closely associated with the STJ that represents an important mechanism driving the stratosphere intrusion. A strong vertical wind shear near the core of STJ is responsible for a large-scale subsidence which brings O_3-enriched air from stratosphere downward to the troposphere. The interaction between the subsidence extended from 100 hPa to 600 hPa and then updraft airflow rises from surface to 600 hPa lead to the large O_3 jump at the bottom of the entrainment zone (i.e., 2-2.6km).

The process analysis method was used to quantify the contributions of individual process to the O_3 enhancement in the lower troposphere. Even though the horizontal transport shows a negative contribution, Hong Kong was highly affected by the vertical transport with average contributions of 17.3 ppbv·hr^{-1}, 11.0 ppbv·hr^{-1}, 22.0 ppbv·hr^{-1} corresponding to the positive net O_3 change at different intervals (i.e. 2.6-4 km, 4-10 km, 10-16 km), respectively. Our results indicated that vertical transport was the largest positive contributor to the O_3 enhancement during the stratosphere intrusion event.

This study fills the knowledge gap concerning the source of the O_3 enhancement in the lower troposphere in Hong Kong during springtime, particularly the quantification of contribution of the stratosphere intrusion to high O_3. It strongly denotes that besides the transport of biomass burning to the spring O_3 maximum, the contribution of the stratosphere intrusion played an important role, and needs to be further considered and well-studied with more attentions. Thus, more observations and modeling studies are advised to further investigate stratospheric intrusions influenced O_3 events versus biomass burning aged plumes influencing surface O_3.

Declaration of Competing Interest

None.

Acknowledgement

The research was supported jointly by the National Natural Science Foundation of China (No. 91644221), the Xianyang major science and technology projects (2017K01-35), China, and was partially supported by start-up foundation (163108094) from Nanjing Forestry University.

Appendix A. Supplementary data

Supplementary data to this article can be found online at https://doi.org/10.1016/j.atmosres.2020.105158.

References

Shapiro, M., 1980. Turbulent Mixing within Tropopause Folds as a Mechanism for the Exchange of Chemical Constituents between the Stratosphere and Troposphere. J. Atmos. Sci. 37 (5), 994–1004.

Ainsworth, E., Yendrek, C., Sitch, S., Collins, W., Emberson, L., 2012. The Effects of Tropospheric Ozone on Net Primary Productivity and Implications for Climate Change. Annu. Rev. Plant. Biol. 63, 637–661. https://doi.org/10.1146/annurev-arplant-042110-103829.

Ambaum, M., 1997. Isentropic Formation of the Tropopause. J. Atmos. Sci. 54, 555–568. https://doi.org/10.1175/1520-0469(1997)054<0555:IFOTT>2.0.CO;2.

Archer, C.L., Caldeira, K., 2008. Historical trends in the jet streams. Geophys. Res. Lett. 35, L8803.

Baray, J.L., Duflot, V., Posny, F.O., Cammas, J.P., Thompson, A.M., Gabarrot, F., Bonne, J.L., Zeng, G., 2012. One year ozonesonde measurements at Kerguelen Island (49.2Â°S, 70.1Â°E): Influence of stratosphere-to-troposphere exchange and long-range transport of biomass burning plumes. J. Geophys. Res-Atmos 117.

Barrett, B.S., Raga, G.B., Retama, A., Leonard, C., 2019. A multi-scale analysis of the tropospheric and stratospheric mechanisms leading to the March 2016 extreme surface ozone event in Mexico City. J. Geophys. Res-Atmos. 8, 4782–4799. https://doi.org/10.1029/2018JD029918.

Barth, M.C., Lee, J., Boxe, C.S., Worden, J., Hodzic, A., 2012. Thunderstorms and upper troposphere chemistry during the early stages of the 2006 North American Monsoon.

Beekmann, M., Ancellet, G., Blonsky, S., Muer, D., Ebel, A., Elbern, H., Hendricks, J., Kowol, J., Mancier, C., Sladkovic, R., Smit, H., Speth, P., Trickl, T., Haver, P., 1997. Regional and Global Tropopause Fold Occurrence and Related Ozone Flux Across the Tropopause. J. Atmos. Chem. 28, 29–44. https://doi.org/10.1023/A:1005897314623.

Blackmon, M.L., Wallace, J.M., Lau, N.C., Mullen, S.L., 1977. An Observational Study of the Northern Hemisphere Wintertime Circulation. J. Atmos. Sci. 34, 1040–1053.

Blake, J.N., 2003. NMHCs and halocarbons in Asian continental outflow during the Transport and Chemical Evolution over the Pacific (TRACE-P) Field Campaign: Comparison With PEM-West B. J. Geophys. Res-Atmos. 108, 8806.

Brasseur, G.P., Kiehl, J.T., Müller, J.F.O., Schneider, T., Granier, C., Tie, X.X., Hauglustaine, D., 1998. Past and future changes in global tropospheric ozone: Impact on radiative forcing. Geophys. Res. Lett. 25, 3807–3810.

Brioude, J., Cammas, J.P., Zbinden, R.M., Thouret, V., 2007. Evidence of tropospheric layering: interleaved stratospheric and planetary boundary layer intrusions. Atmos. Chem. Discuss. 7, 1119–1142.

Büker, M.L., Hitchman, M.H., Tripoli, G.J., Pierce, R.B., Browell, E.V., Avery, M.A., 2005 Resolution dependence of cross-tropopause ozone transport over East Asia. J. Geophys. Res., 110, D03107. doi:10.1029/2004JD004739.

Chan, C.Y., Chan, L.Y., 2000. Effect of meteorology and air pollutant transport on ozone episodes at a subtropical coastal Asian city, Hong Kong. J. Geophys. Res-Atmos. 105, 20707–20724. https://doi.org/10.1029/2000JD900140.

Chan, C.K., Yao, X., 2008. Air pollution in mega cities in China. Atmos. Environ. 42, 1–42. https://doi.org/10.1016/j.atmosenv.2007.09.003.

Chan, L.Y., Liu, H.Y., Lam, K.S., et al., 1998. Analysis of the seasonal behavior of tropospheric ozone at Hong Kong. Atmos. Environ. 32 (2), 159–168.

Chan, L.Y., Chan, C.Y., Liu, H.Y., Christopher, S., Oltmans, S.J., Harris, J.M., 2000. A case study on the biomass burning in southeast Asia and enhancement of tropospheric ozone over Hong Kong. Geophys. Res. Lett. 27, 1479–1482.

Chan, C., Chan, L.Y., Harris, J.M., Oltmans, S., Blake, D.R., Qin, Y., Zheng, Y., Zheng, X.D., 2003. Characteristics of biomass burning emission sources, transport, and chemical speciation in enhanced springtime tropospheric ozone profile over Hong Kong. J. Geophys. Res-Atmos. 108. https://doi.org/10.1029/2001JD001555.

Chou, M., 1995. An Efficient Thermal Infrared Radiation Parameterization For Use In General Circulation Models. NASA Tech. Memo, pp. 3.

Chuang, M.T., Zhang, Y., Kang, D., 2011. Application of WRF/Chem-MADRID for real-time air quality forecasting over the Southeastern United States. Atmos. Environ. 45, 6241–6250.

Collins, W.J., Derwent, R.G., Johnson, C.E., Stevenson, D.S., 2000. The impact of human activities on the photochemical production and destruction of tropospheric ozone. Q. J. Roy. Meteor. Soc. 126, 1925–1951.

Considine, D., Logan, J., Olsen, M., 2008. Evaluation of near-tropopause ozone distributions in the Global Modeling Initiative combined stratosphere/troposphere model with ozonesonde data. Atmos. Chem. Phys. Discuss. 8, 1589–1634.

Cooper, S.M., Peterson, D.L., 2000. Spatial distribution of tropospheric ozone in western Washington. USA. Environ. Pollut. 107 (3), 339–347.

Cooper, O.R., Parrish, D.D., Stohl, A., Trainer, M., Nédélec, P., Thouret, V., Cammas, J.P., Oltmans, S.J., Johnson, B.J., Tarasick, D., 2010. Increasing springtime ozone mixing ratios in the free troposphere over western North America. Nature. 463, 344–348.

Derwent, G.R., 1990. Evaluation of a number of chemical mechanisms for their application in models describing the formation of photochemical ozone in Europe. Atmos. Environ., part A.general Topics 24, 2615–2624.

Derwent, R.G., Stevenson, D.S., Collins, W.J., Johnson, C.E., 2004. Intercontinental transport and the origins of the ozone observed at surface sites in Europe. Atmos. Environ. 38, 1891–1901. https://doi.org/10.1016/j.atmosenv.2004.01.008.

Dickinson, R.E., Cicerone, R.J., 1986. Future global warming from atmospheric trace gases. Nature. 319, 109–115. https://doi.org/10.1038/319109a0.

Dragani, R., 2011. On the quality of the ERA-Interim ozone reanalyses: comparisons with satellite data. Q. J. Roy. Meteor. Soc. 137, 1312–1326.

Emmons, L.K., A.E.C.L, 2010. Impact of Mexico City emissions on regional air quality from MOZART-4 simulations. Atmos. Chem. Phys. 10, 6195–6212.

Fast, J.D., Allan, J., Bahreini, R., Craven, J., Emmons, L., Ferrare, R., Hayes, P.L., Hodzic, A., Holloway, J., Hostetler, C., Jimenez, J.L., Jonsson, H., Liu, S., Liu, Y., Metcalf, A., Middlebrook, A., Nowak, J., Pekour, M., Perring, A., Zhang, Q., 2014. Modeling regional aerosol variability over California and its sensitivity to emissions and long-range transport during the 2010 CalNex and CARES campaigns. Atmos. Chem. Phys. Discuss. 14, 7187–7303. https://doi.org/10.5194/acpd-14-7187-2014.

Fishman, J., Crutzen, P.J., 1978. The origin of ozone in the troposphere. Nature. 274, 855–858.

Frédéric, Hourdin, Foujols, M.A., Codron, F., et al., 2013. Impact of the LMDZ atmospheric grid configuration on the climate and sensitivity of the IPSL-CM5A coupled model. Climate Dynamics. 40 (9-10), 2167–2192.

Ganguly, D.N., 2012. Influence of Stratospheric Intrusion on the Surface Ozone Levels in India. Isrn. Meteor. 2012, 1–7.

Gao, J., Zhu, B., Xiao, H., Kang, H., Hou, X., Shao, P., 2016. A case study of surface ozone source apportionment during a high concentration episode, under frequent shifting wind conditions over the Yangtze River Delta. China. Sci. Total Environ. 544, 853–863.

Gaudel, A., Ancellet, G., Godin-Beekmann, S., 2015. Analysis of 20 years of tropospheric ozone vertical profiles by lidar and ECC at Observatoire de Haute Provence (OHP) at 44°N, 6.7°E. Atmos. Environ 113. https://doi.org/10.1016/j.atmosenv.2015.04.028.

Gettelman, A., Holton, J.R., Rosenlof, K.H., 1997. Mass fluxes of O3, CH4, N2O and CF2Cl2 in the lower stratosphere calculated from observational data. J. Geophys. Res-Atmos. 102.

Gouget, H., Cammas, J.P., Marenco, A., Rosset, R., JonquièRes, I., 1996. Ozone peaks associated with a subtropical tropopause fold and with the trade wind inversion: A case study from the airborne campaign TROPOZ II over the Caribbean in winter. J. Geophys. Res. 101, 25979. https://doi.org/10.1029/96JD01545.

Greenslade, J.W., Alexander, S.P., Schofield, R., Fisher, J.A., Klekociuk, A.K., 2017. Stratospheric ozone intrusion events and their impacts on tropospheric ozone. Atmos. Chem. Phys. 1-28.

Grell, G.A., Peckham, S.E., Schmitz, R., Mckeen, S.A., Eder, B., 2005. Fully coupled "online" chemistry in the WRF model. Atmos. Environ. 39, 6957–6975.

Griffiths, P.T., Keeble, J., Shin, Y.M., Abraham, N.L., Archibald, A.T., Pyle, J.A., 2020. On the Changing Role of the Stratosphere on the Tropospheric Ozone Budget: 1979–2010. Geophys. Res. Lett. 47. https://doi.org/10.1029/2019GL086901.

Hegglin, M.I., Shepherd, T.G., 2009. Large climate-induced changes in ultraviolet index and stratosphere-to-troposphere ozone flux. Nat. Geosci. 2, 687–691.

Hoell, J.M., Davis, D.D., Liu, S.C., Newell, R.E., Akimoto, H., McNeal, R.J., Bendura, R.J., 1997. The Pacific Exploratory Mission-West Phase B: February-March, 1994. J. Geophys. Res-Atmos. 102, 28223.

Holton, J.R., Haynes, P.H., McIntyre, M.E., Douglass, A.R., Rood, R.B., Pfister, L., 1995. Stratosphere-troposphere exchange. Rev. Geophys. 33, 403–439.

Hong, S., Noh, Y., Dudhia, J., 2006. A New Vertical Diffusion Package with an Explicit Treatment of Entrainment Processes. Mon. Wwather. Rev. 134. https://doi.org/10.1175/MWR3199.1.

Horowitz, L., 2003. A global simulatin of tropospheric ozone and related tracers: Description and evalation of MOZART, version 2. J. Geophys. Res. 108.

Hsu, J., Prather, M.J., Wild, O., 2005. Diagnosing the stratosphere-to-troposphere flux of ozone in a chemistry transport model. J. Geophys. Res-Atmos. 110.

Hu, C., Griffis, T.J., Baker, J.M., Wood, J.D., Millet, D.B., Lee, X., 2019. Modeling the sources and transport processes associated with extreme ammonia episodes in the US Corn Belt. J. Geophys. Res. https://doi.org/10.1029/2019JD031207.

Huang, J., 2005. Numerical simulation and process analysis of typhoon-related ozone episodes in Hong Kong. J. Geophys. Res. 110. https://doi.org/10.1029/2004JD004914.

Iwabe, C.M.N., D.R.R.P, 2009. An event of stratospheric air intrusion and its associated secondary surface cyclogenesis over the South Atlantic Ocean. J. Geophys. Res-Atmos. 114. https://doi.org/10.1029/2008JD011119.

Jacob, D.J., Logan, J.A., Murti, P.P., 1999. Effect of rising Asian emissions on surface ozone in the United States. Geophys. Res. Lett. 26, 2175–2178. https://doi.org/10.1029/1999GL900450.

Jeffries, H.E., Tonnesen, S., 1994. A comparison of two photochemical reaction mechanisms using mass balance and process analysis. Atmos. Environ. 28, 2991–3003. https://doi.org/10.1016/1352-2310(94)90345-X.

Kim, J.H., Lee, H., 2010. What Causes the Springtime Tropospheric Ozone Maximum over Northeast Asia? Adv. Atmos. Sci. 27, 543–551.

Kim, Y.K., Lee, H.W., Park, J., Moon, Y.S., 2002. The stratosphere–troposphere exchange of ozone and aerosols over Korea. Atmos. Environ. 36, 449–463. https://doi.org/10.1016/S1352-2310(01)00370-3.

Kim, Y., Sartelet, K., Seigneur, C., 2009. Comparison of two gas-phase chemical kinetic mechanisms of ozone formation over Europe. J. Atmos. Chem. 62, 89–119. https://doi.org/10.1007/s10874-009-9142-5.

Komhyr, W., Oltmans, S., Chopra, A., Franchois, P., 1985. Performance Characteristics of High-Altitude ECC Ozonesondes. https://doi.org/10.1007/978-94-009-5313-0_100.

Komhyr, W., Oltmans, S., Franchois, P., Evans, W., Matthews, W., 1989. The Latitudinal Distribution of Ozone to 35 Km Altitude from ECC Ozonesonde Observatons, 1985-1987.

Krishnamurti, T., 1961. The Subtropical Jet Stream of Winter. J. Atmos. Sci. 18, 172–191. https://doi.org/10.1175/1520-0469(1961)018<0172:TSJSOW>2.0.CO;2.

Krupa, S.V., Manning, W.J., 1988. Atmospheric ozone: formation and effects on vegetation. Environ. Pollut. 50, 101–137. https://doi.org/10.1016/0269-7491(88)90187-x.

Lacis, A., Wuebbles, D., Logan, J., 1990. Radiative forcing by changes in the vertical distribution of ozone. J. Geophys. Res-Atmos. 95. https://doi.org/10.1029/JD095iD07p09971.

Lam, K.S., Wang, T.J., Wu, C.L., Li, Y.S., 2005. Study on an ozone episode in hot season in Hong Kong and transboundary air pollution over Pearl River Delta region of China. Atmos. Environ. 39, 1967–1977.

Lamarque, J.F., Emmons, L.K., Hess, P.G., Kinnison, D.E., Tilmes, S., Vitt, F., Heald, C.L., Holland, E.A., Lauritzen, P.H., Neu, J., Orlando, J.J., Rasch, P.J., Tyndall, G.K., 2012. CAM-chem: description and evaluation of interactive atmospheric chemistry in the Community Earth System Model. Geosci. Model. Dev. 5, 369–411. https://doi.org/10.5194/gmd-5-369-2012.

Langford, A., 1999. Stratosphere-troposphere exchange at the subtropical jet: Contribution to the tropospheric ozone budget at midlatitudes. Geophys. Res. Lett 26. https://doi.org/10.1029/1999GL900556.

Langford, A., Brioude, J., Cooper, O., Senff II, C., Hardesty, R., Johnson, B., Oltmans, S., 2012. Stratospheric influence on surface ozone in the Los Angeles area during late spring and early summer of 2010. J. Geophys. Res. 117. https://doi.org/10.1029/2011JD016766.

Lanzendorf, E.J., Hanisco, T.F., Wennberg, P.O., Cohen, R.C., Bui, T.P., 2001. Establishing the Dependence of [HO2]/[OH] on Temperature, Halogen Loading, O3, and NOx Based on in Situ Measurements from the NASA ER-2. J.Phys.Chem.A 105, 1535–1542.

Lei, S., Min, X., Tijian, W., Pulong, C., Yong, H., Shu, L., Bingliang, Z., Mengmeng, L., Da, G., 2016. Integrated studies of a regional ozone pollution synthetically affected by subtropical high and typhoon system in the Yangtze River Delta region. China. Atmos. Chem. Phys. 1-32.

Levelt, P.F., van den Oord, G.H.J., Dobber, M.R., Malkki, A., Visser, H., de Vries, J., Saari, H., 2006. The Ozone Monitoring Instrument. Ieee. T. Geosci. Remote. 44, 1093–1101. https://doi.org/10.1109/TGRS.2006.872333.

Li, D., Bian, J., 2015. Observation of a Summer Tropopause Fold by Ozonesonde at Changchun,China: Comparison with Reanalysis and Model Simulation. Adv. Atmos. Sci. 032, 1354–1364.

Li, M., Zhang, Q., Kurokawa, J., Woo, J.H., He, K.B., Lu, Z., Ohara, T., Song, Y., Streets, D.G., Carmichael, G.R., 2015. MIX: a mosaic Asian anthropogenic emission inventory for the MICS-Asia and the HTAP projects. Atmos. Chem. Phys. Discuss. 15, 34813–34869.

Liang, Q., Jaegle, L., Jaffe, D., Weiss, P., Mcclintick, A., Snow, J., 2002. Seasonal variations in long-range transport and its influence on CO and Ozone levels in the northeastern Pacific. AGU Fall Meeting.

Liang, Q., Jaeglé, L., Jaffe, D.A., Weiss Penzias, P., Heckman, A., Snow, J.A., 2004. Long-range transport of Asian pollution to the northeast Pacific: Seasonal variations and transport pathways of carbon monoxide. J. Geophys. Res-Atmos. 109.

Lin, Y., Farley, R., Orville, H., 1983. Bulk Parameterization of the Snow Field in a Cloud Model. J. Appl. Meteorol. 22, 1065–1092. https://doi.org/10.1175/1520-0450(1983)022<1065:BPOTSF>2.0.CO;2.

Lin, M., Fiore, A.M., Cooper, O.R., Horowitz, L.W., Langford, A.O., Levy II, H., Johnson, B.J., Naik, V., Oltmans, S.J., Senff, C.J., 2012. Springtime high surface ozone events over the western United States: Quantifying the role of stratospheric intrusions. J. Geophys. Res 117, D00V22. https://doi.org/10.1029/2012JD018151.

Ling, Z.H., Guo, H., Zheng, J.Y., Louie, P.K.K., Cheng, H.R., Jiang, F., Cheung, K., Wong, L.C., Feng, X.Q., 2013. Establishing a conceptual model for photochemical ozone pollution in subtropical Hong Kong. Atmos. Environ. 76, 208–220. https://doi.org/10.1016/j.atmosenv.2012.09.051.

Liu, Z., Roy, S.S., 2015. Spatial Patterns of Seasonal Level Diurnal Variations of Ozone and Respirable Suspended Particulates in Hong Kong. Prof. Geogr. 67, 17–27.

Liu, X., Kutzbach, J., Liu, Z., An, Z., Li, J., 2003. The Tibetan Plateau as amplifier of orbital-scale variability of the East Asian monsoon. Geophys. Res. Lett. 30. https://doi.org/10.1029/2003GL017510.

Locatelli, R., Bousquet, P., Hourdin, F., et al., 2015. Atmospheric transport and chemistry of trace gases in LMDz5B: evaluation and implications for inverse modelling. Geosci. Model. Dev. 8, 129–150.

Logan, J.A., 1989. Ozone in rural areas of the United States. J. Geophys. Res-Atmos. 94.

Meul, S., Langematz, U., Kröger, P., Oberländer-Hayn, S., Jöckel, P., 2018. Future changes in the stratosphere-to-troposphere ozone mass flux and the contribution from climate change and ozone recovery. Atmos. Chem. Phys. 1-46.

Mickley, L.J., Jacob, D.J., Rind, D., 2001. Uncertainty in preindustrial abundance of tropospheric ozone: Implications for radiative forcing calculations. J. Geophys. Res-Atmos. 106, 3389.

Mlawer, E.J., Taubman, S.J., Brown, P.D., Iacono, M.J., Clough, S.A., 1997. Radiative transfer for inhomogeneous atmospheres: RRTM, a validated correlated-k model for the longwave. J. Geophys. Res-Atmos. 102, 16663–16682. https://doi.org/10.1029/97JD00237.

Moody, J., Oltmans, S., Levy, H., Merrill, J., 1995. Transport climatology of tropospheric ozone: Bermuda, 1988-1991. J. Geophys. Res. 100, 7179–7194. https://doi.org/10.1029/94JD02830.

Oh, I., Kim, Y., Hwang, M., Kim, C., Kim, S., Song, S., 2010. Elevated Ozone Layers over the Seoul Metropolitan Region in Korea: Evidence for Long-Range Ozone Transport from Eastern China and Its Contribution to Surface Concentrations. J. Appl. Meteorol. Clim. 49, 203–220. https://doi.org/10.1175/2009JAMC2213.1.

Olsen, M.A., Gallus, W.A., Stanford, J.L., Brown, J.M., 2000. Fine-scale comparison of TOMS total ozone data with model analysis of an intense Midwestern cyclone. J. Geophys. Res-Atmos. 105.

Oltmans, S., Johnson, B., Harris, J., Thompson, A., Liu, H., Voemel, H., Chan, C., Fujimoto, T., Brackett, V., Chang, W.L., Chen, J., 2003. Tropospheric Ozone Over the North Pacific from Ozonesdonde Observations. J. Geophys. Res. 109. https://doi.org/10.1029/2003JD003466.

Ott, L.E., Duncan, B.N., Thompson, A.M., Diskin, G., Fasnacht, Z., Langford, A.O., Yoshida, Y., 2016. Frequency and impact of summertime stratospheric intrusions over Maryland during DISCOVER-AQ (2011): New evidence from NASA's GEOS-5 simulations. J. Geophys. Res. 121, 3687–3706. https://doi.org/10.1002/2015JD024052.

Penkett, S.A., Evans, M.J., Reeves, C.E., Law, K.S., Monks, P.S., Bauguitte, S.J.B., Pyle, J.A., Green, T.J., Bandy, B.J., Mills, G., Cardenas, L.M., Barjat, H., Kley, D., Schmitgen, S., Kent, J.M., Dewey, K., Methven, J., 2004. Long-range transport of ozone and related pollutants over the North Atlantic in spring and summer. Atmos. Chem. Phys. Discuss. 4, 4407–4454. https://doi.org/10.5194/acpd-4-4407-2004.

Pfister, G.G., Reddy, P., Barth, M.C., Flocke, F.F., Fried, A., Herndon, S.C., Sive, B.C., Sullivan, J.T., Thompson, A.M., Yacovitch, T.I., 2017. Using observations and source specific model tracers to characterize pollutant transport during FRAPPé and DISCOVER-AQ. J. Geophys. Res-Atmos.

Price, J.D., Vaughan, G., 1993. The potential for stratosphere-troposphere exchange in cut-off-low systems. Q. J. Roy. Meteor. Soc. 119, 343–365.

Price, J.D., Howells, A., Vaughan, G., 1994. Removal of meteorological synoptic-scale disturbances from TOMS total ozone fields. Geophys. Res. Lett. 21, 1475–1478.

Pu, X., Wang, T.J., Huang, X., Melas, D., Zanis, P., Papanastasiou, D.K., Poupkou, A., 2017. Enhanced surface ozone during the heat wave of 2013 in Yangtze River Delta region. China. Sci. Total. Environ. 603, 807–816.
Reed, R.J., 1955. a Study of a Characteristic Tpye of Upper-Level Frontogenesis. J. Atmos. Sci. 12, 226–237.
Regener, V.H., 1957. The vertical flux of atmospheric ozone. J. Geophys. Res. 62.
Ren, R., Wu, G., Cai, M., Shuyue, S., Liu, X., Li, W., 2014. Progresses in Stratosphere-Troposphere Interactions: Application of Isentropic Potential Vorticity Dynamics and Effect of the Tibetan Plateau. J. Meteor. Res. 28, 714–731. https://doi.org/10.1007/s13351-014-4026-2.
Richter, A., Burrows, J.P., Nü, H., Granier, C., Niemeier, U., 2005. Increase in tropospheric nitrogen dioxide over China observed from space. Nature. 437, 129–132.
Schoeberl, M., 2003. Extratropical Stratosphere-Troposphere Mass Exchange. J. Geophys. Res. 109. https://doi.org/10.1029/2004JD004525.
Sillman, S., 1995. The use of NOy, H2O2, and HNO3 as indicators for ozone-NOx- hydrocarbon sensitivity in urban locations. J. Geophys. Res. 100, 175–188.
Sillman, S., 2014. Tropospheric Ozone and Photochemical Smog. Treatise Geochem. 9, 407–431.
Sillman, S., Logan, J.A., Wofsy, S.C., 1990. The sensitivity of ozone to nitrogen oxides and hydrocarbons in regional ozone episodes. J. Geophys. Res-Atmos. 95, 1837–1851.
Singh, R.B., Sloan, J.J., 2006. A high-resolution NOx emission factor model for North American motor vehicles. Atmos. Environ. 40, 5214–5223. https://doi.org/10.1016/j.atmosenv.2006.04.012.
Skerlak, B., Sprenger, M., Wernli, H., 2014. A global climatology of stratosphere-troposphere exchange using the ERA-Interim data set from 1979 to 2011. Atmos. Chem. Phys. 14, 913–937. https://doi.org/10.5194/acp-14-913-2014.
Sørensen, J.H., Nielsen, N.W., 2001. Intrusion of stratospheric ozone to the free troposphere through tropopause folds - A case study. Phys. Chem. Earth. Pt. B. 26, 801–806.
Stevenson, D.S., Dentener, F.J., Schultz, M.G., Ellingsen, K., Noije, T.V., Coauthors, 2006. Multimodel ensemble simulations of present-day and near-future tropospheric ozone. 111. pp. 263–269.
Stohl, A., 2001. A 1-year Lagrangian "climatology" of airstreams in the Northern Hemisphere troposphere and lowermost stratosphere. J. Geophys. Res. 106, 7263–7280. https://doi.org/10.1029/2000JD900570.
Stohl, A., Bonasoni, P., Cristofanelli, P., Collins, W., 2003. Stratosphere-troposphere exchange: A review, and what we have learned from STACCATO. J. Geophys. Res. 108, 8516. https://doi.org/10.1029/2002JD002490.
Sudo, Kengo, 2003. Future changes in stratosphere-troposphere exchange and their impacts on future tropospheric ozone simulations. Geophys. Res. Lett. 30, 2256.
Sudo, K., Takahashi, M., Kurokawa, J., Akimoto, H., 2002. CHASER: A global chemical model of the troposphere 1. Model description. J. Geophys. Res. 107. https://doi.org/10.1029/2001JD001113.
Tang, Q., Prather, M., Hsu, J., 2011. Stratosphere-troposphere exchange ozone flux related to deep convection. Geophys. Res. Lett. 38. https://doi.org/10.1029/2010GL046039.
Vieno, M., Dore, A.J., Doherty, R., Heal, M., Reis, S., Hallsworth, S., Tarrasón, L., Wind, P., Sutton, M., 2008. Modelling surface ozone during the 2003 heat wave in the UK. Hrvatski Meteoroloski Casopis. 43, 83–87.
Wang, T., Wei, X.L., Ding, A.J., Poon, C.N., Lam, K.S., Li, Y.S., Chan, L.Y., Anson, M., 2009. Increasing surface ozone concentrations in the background atmosphere of Southern China, 1994–2007. Atmos. Chem. Phys. 9, 6217–6227. https://doi.org/10.5194/acp-9-6217-2009.
Westervelt, D., Ma, C., He, M., Fiore, A., Kinney, P., Kioumourtzoglou, M., Wang, S., Xing, J., Dian, D., Correa, G., 2019. Mid-21st century ozone air quality and health burden in China under emissions scenarios and climate change. Environ. Res. Lett. 14. https://doi.org/10.1088/1748-9326/ab260b.
Wild, O., Zhu, X., Prather, M.J., 2000. Fast-J: Accurate Simulation of In- and Below-Cloud Photolysis in Tropospheric Chemical Models. J. Atmos. Chem. 37, 245–282. https://doi.org/10.1023/A:1006415919030.
Yang, H., Chen, G., Tang, Q., Hess, P., 2016. Quantifying Isentropic Stratosphere-Troposphere Exchange of Ozone. J. Geophys. Res-Atmos. 121.
Young, P.J., Archibald, A.T., Bowman, K.W., Lamarque, J.F., Naik, V., Stevenson, D.S., Tilmes, S., Voulgarakis, A., Wild, O., Bergmann, D., Cameron-Smith, P., Cionni, I., Collins, W.J., Ren, S.B.D., Doherty, R.M., Eyring, V., Faluvegi, G., Horowitz, L.W., Josse, B., Lee, Y.H., MacKenzie, I.A., Nagashima, T., Plummer, D.A., Righi, M., Rumbold, S.T., Skeie, R.B., Shindell, D.T., Strode, S.A., Sudo, K., Szopa, S., Zeng, G., 2013. Pre-industrial to end 21st century projections of tropospheric ozone from the Atmospheric Chemistry and Climate Model Intercomparison Project (ACCMIP). Atmos. Chem. Phys. Discuss. 13, 2063–2090.
Zanis, P., Hadjinicolaou, P., Dafka, S., Tyrlis, E., Lelieveld, J., 2013. The summertime free tropospheric ozone pool over Eastern Mediterranean/Middle East. Atmos. Chem. Phys. Disscuss. 14, 1304.
Zhang, Y., Liu, H., Crawford, J.H., Considine, D.B., Chan, C., Oltmans, S.J., Thouret, V., 2012. Distribution, variability and sources of tropospheric ozone over south China in spring: Intensive ozonesonde measurements at five locations and modeling analysis. J. Geophys. Res-Atmos. 117.
Zhang, Y., Cooper, O.R., Gaudel, A., Thompson, A.M., Nédélec, P., Ogino, S., West, J.J., 2016. Tropospheric ozone change from 1980 to 2010 dominated by equatorward redistribution of emissions. Nat. Geosci. 9, 875–879. https://doi.org/10.1038/ngeo2827.
Zhao, K., Bao, Y., Huang, J., Wu, Y., Moshary, F., Arend, M., Wang, Y., Lee, X., 2019. A high-resolution modeling study of a heat wave-driven ozone exceedance event in New York City and surrounding regions. Atmos Environ. 199, 368–379.
Zhou, D., Ding, A., Mao, H., Fu, C., Tao, W., Chan, L., Ding, K., Zhang, Y., Liu, J., An, L., Hao, N., 2013. Impacts of the East Asian monsoon on lower tropospheric ozone over coastal South China Impacts of the East Asian monsoon on lower tropospheric ozone over coastal South China. Environ. Res. Lett. 8, 44011–44017. https://doi.org/10.1088/1748-9326/8/4/044011.